

Remote Sensing of Ocean Waters with Raman and Brillouin Scattering

Joyanto Mukerjee

DSTO-TN-0346

DISTRIBUTION STATEMENT A
Approved for Public Release
Distribution Unlimited

Remote Sensing of Ocean Waters with Raman and Brillouin Scattering

Joyanto Mukerjee

Maritime Operations Division
Aeronautical and Maritime Research Laboratory

DSTO-TN-0346

ABSTRACT

This document presents a literature survey on the remote sensing of ocean waters with Raman and Brillouin scattering. It explains the physical process involved for these scattering processes to occur in water and a description of techniques employed by researchers to exploit Raman and Brillouin scattering to measure temperature and sound velocity in water. The papers surveyed for this report present measurement accuracies ranging from ± 0.75 m/sec to ± 10 m/sec for measuring sound velocity using Brillouin scattering and ± 0.4 °C to 2 °C for measuring temperature using Raman scattering.

20010814 023

RELEASE LIMITATION

Approved for public release

DEPARTMENT OF DEFENCE
DEFENCE SCIENCE & TECHNOLOGY ORGANISATION

DSTO

AQ F01-11-2324

Published by

*DSTO Aeronautical and Maritime Research Laboratory
506 Lorimer St
Fishermans Bend Vic 3207 Australia*

Telephone: (03) 9626 7000

Fax: (03) 9626 7999

© Commonwealth of Australia 2001

AR-011-826

March 2001

APPROVED FOR PUBLIC RELEASE

Remote Sensing of Ocean Waters with Raman and Brillouin Scattering

Executive Summary

This document has been prepared as a literature survey of Raman and Brillouin scattering in water. It is intended to be used as a reference for determining future direction of DSTO research in this field.

This report describes the mechanisms of Raman and Brillouin scattering, the current methods for detection and the limits of their accuracy and sensitivity.

This literature survey discusses researchers' contributions on the measurement in water of sound velocity and temperature using Raman and Brillouin scattering. Raman or Brillouin scattering of laser light in seawater provide mechanisms for remote sensing of water properties, which could be used for military purposes. Researchers have reported results with accuracies ranging from ± 0.75 m/s to ± 10 m/sec for measuring sound speed using Brillouin scattering and $\pm 0.4^{\circ}\text{C}$ to $\pm 2^{\circ}\text{C}$ for measuring temperature using Raman scattering.

A brief discussion of the possible applications of these techniques includes:

- An alternative temperature profiling capability to expendable bathythermographs. Maritime platforms could use a lidar system, which is ready to use at the press of a button for gathering velocity and temperature profiles. This can be repeated many times because the lidar probes the water with laser light instead of a physical transducer that is lost after one measurement.
- Depending on the sensitivity a temperature profiling lidar may be used to detect the presence of submerged vehicles by tracking thermal changes induced in the water column.

Contents

1. INTRODUCTION	1
2. BRILLOUIN SCATTERING	2
2.1 The Brillouin Scattering Process.....	2
2.2 Precision and Sensitivity using Brillouin Scattering.....	3
2.3 Brillouin Measurement Techniques	5
2.4 Remote Sensing of Brillouin Scattering.....	7
3. RAMAN SCATTERING	11
3.1 The Raman Scattering Process	11
3.2 Raman Measurement Techniques	13
3.2.1 Two-colour Technique.....	13
3.2.2 Depolarisation Technique	15
3.3 Precision and Sensitivity.....	17
3.4 Summary of Reported Results	18
3.5 Remote Sensing of Raman Scattering.....	19
4. CONCLUSION	20
5. REFERENCES.....	22
6. BIBLIOGRAPHY	24
APPENDIX A: BRILLOUIN FREQUENCY SHIFT	25

1. Introduction

When light propagates through water it can be elastically and inelastically scattered. Elastic scattering is a process in which light is reflected upon colliding with molecules and particulates that make up the body of water. When light is elastically scattered it does not experience a wavelength change. Elastic scattering between a light particle (photon) and water molecules and particulates can be approximated in the macroscopic world by the behaviour of billiard balls when they collide with each other. Rayleigh scattering is an example of light that is elastically scattered from water. The blue colour of the sky is a result of Rayleigh scattering taking place in the upper atmosphere. The blue colour results because scattering is wavelength dependent. Tyndall scattering is defined by Hirschberg et al (1975) as elastic scattering of light from particulates suspended in water. The definition of Tyndall scattering also includes Mie scattering which is a result of light back scattering from an elastic collision with particulates suspended in water.

Inelastic scattering of light is defined as an event in which an incident light field is absorbed and then re-emitted at an energy level that is more or less than the incident energy level. Many collisions that we observe in the macroscopic world are inelastic collisions. Vehicle collisions are an example of this, if two vehicles collided elastically they would simply bounce off one another like billiard balls. Instead the energy in the collision goes into moving and deforming the vehicles and producing acoustic and heat energy.

When a light field interacts inelastically with water it can gain or lose energy. This translates to observing a change in the perceived colour (wavelength) of a light field after an inelastic collision. The size of the change depends upon the type of inelastic scattering that a light field experiences. The two inelastic scattering processes of light in water are known as Brillouin and Raman scattering. This report presents a review of Brillouin and Raman scattering for optical remote sensing of ocean properties.

2. Brillouin Scattering

2.1 The Brillouin Scattering Process

The velocity of sound in water is a function of temperature and salinity. Brillouin scattering provides a direct measure of the velocity of sound in water. Therefore the temperature of a water sample can be measured by exploiting the Brillouin scattering process coupled with salinity data. If Brillouin backscatter is measured using a range-resolved system then the velocity and temperature profile can be determined for a column of water. This has significant implications for hydrographic sciences, meteorology and for sonar processing onboard military platforms.

The physical phenomenon is a result of photon-phonon interaction. A phonon is a quantum of acoustic radiation, which propagates through the water at the speed of sound. A photon is a quantum of electromagnetic radiation travelling at the speed of light. Photons are moving at approximately five orders of magnitude faster than phonons. When the two waves interact, a photon virtually sees a phonon as a static region of hypersonic density fluctuations. These density fluctuations present themselves as a Bragg scatterer and the photon reacts accordingly. Bragg scattering is used to describe the behaviour of light when it interacts with periodic reflection planes. When a photon-phonon interaction takes place the photon sees the phonon as an apparent family of parallel plane reflectors. However since the acoustic waves are moving, doppler shifts are introduced to the reflected light. The Brillouin scattering process is shown in Figure 2.1.

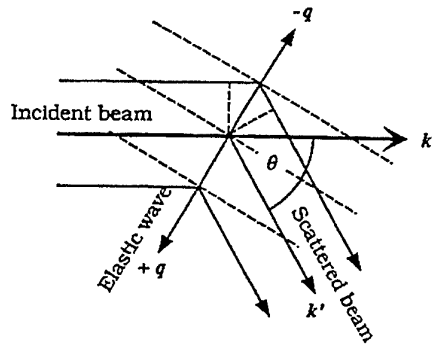


Figure 2.1: An illustration of the Brillouin scattering process taken from Hickman et al (1991) where k and k' are wavenumbers of the incident and scattered beam respectively. The angle θ is the scattering angle and $\pm q$ are wavenumbers representing phonons moving toward and away from the incident beam.

An expression for Brillouin scattering in water has been derived by Hickman et al (1991) to be

$$\frac{\Delta \nu_B}{\nu} = \pm 2n \frac{v_s}{c} \sin\left(\frac{\theta}{2}\right). \quad (1)$$

Where $\Delta \nu_B$ is the frequency shift, ν is the frequency of the laser beam, n is the refractive index of the medium, v_s is velocity of sound, c is the speed of light and θ is the scattering angle. A lidar system that has collection optics co-located and parallel to the direction of the probe laser beam is likely to detect Brillouin scattering at a scattering angle of 180° . The Doppler shift will depend on the direction of travel of a phonon relative to the incident photon. While interacting with randomly created

phonons, there is an equal chance of an incident photon encountering a phonon travelling toward or away from it. Hence the \pm in equation 1 describes the Doppler shifted Brillouin doublet. The frequency doublets are known as anti-Stokes and Stokes frequencies produced by phonons travelling toward or away from incident photons. Figure 2.2 shows a theoretical spectrum of a Brillouin backscattered return. Appendix A presents a plot of the Brillouin shift as a function of sound speed. The refractive index of the medium is assumed to be 1.339 and the scattering angle is assumed to be 180° .

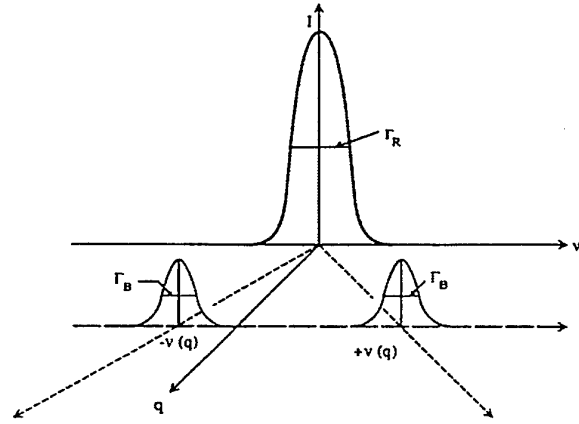


Figure 2.2: This is a theoretical spectrum of a Brillouin backscattered signal. It contains the elastically scattered centre line (some authors refer to it as the Rayleigh line) in between two Brillouin scattered peaks. Γ_R is the full width at half maximum (FWHM) of the Rayleigh line. Γ_B is the FWHM of the Brillouin return. This figure is reproduced from Hickman et al (1991). The ν axis is frequency.

Stimulated Brillouin scattering occurs when the light intensity exceeds a threshold value. It occurs because the photons are creating phonons by locally heating the lattice structure of the water. This results in a backscattered return that is due to a photon giving up some energy to create a phonon. The backscattered spectrum primarily consists of an elastically scattered centre line and a stimulated Brillouin scattering return that is slightly lower in energy and therefore longer in wavelength than the elastically scattered line. To produce sufficient light intensity for stimulated Brillouin scattering the laser must be focussed at a specific depth, making range-resolved profiling systems more complex.

2.2 Precision and Sensitivity using Brillouin Scattering

The key factor limiting precision in measuring sound speed and temperature is reported by Hickman et al (1991) to be the statistical uncertainty of the measured Brillouin shift. Hickman has presented an expression for the fractional root mean square error of equation (1). It is given in terms of the sound velocity to be

$$\frac{\delta v_s}{v_s} = \left[\left(\frac{\delta \nu}{\nu} \right)^2 + \left(\frac{\delta \theta}{2} \cot \frac{\theta}{2} \right)^2 + \left(\frac{\delta n}{n} \right)^2 + \left(\frac{\delta(\Delta \nu_b)}{\Delta \nu_b} \right)^2 \right]^{1/2} \quad (2)$$

Using current laser injection locking techniques the term defining uncertainty in laser frequency is in the order of 10^{-7} and is ignored. For a 180° backscatter system the cot term is zero. The refractive index is a function of salinity and temperature. According to Hickman et al (1991) for temperatures ranging from 0° to 30° the refractive index is more sensitive to salinity. It can introduce a small component into the uncertainty expression but it will be ignored at this stage, primarily to keep the focus on measuring the Brillouin shift. The uncertainty in the refractive index should be included when it is comparable in size to the uncertainty in the Brillouin shift or simply for greater precision. Ignoring the uncertainties in laser frequency, scattering angle and refractive index, equation (2) approximates to

$$\frac{\delta v_s}{v_s} \approx \frac{\delta(\Delta v_B)}{\Delta v_B}. \quad (3)$$

An expression for the statistical uncertainty in the measurement of the Brillouin shift is reported by Hickman to be

$$\delta(\Delta v_B) = \alpha \frac{\Gamma_B}{SNR} \text{ MHz}. \quad (4)$$

Where Γ_B is the Brillouin linewidth (see Figure 2.2) and α is a constant, which depends on the measuring system precision. Emery and Fry (1997) have published experimental results showing the Brillouin linewidth to be 500 MHz. For the purpose of this study the Brillouin linewidth is assumed to be 500 MHz and α is assumed to be unity. N_{pe} is defined in Hickman et al (1991) as the number of output Brillouin photoelectrons produced per pulse by an optical receiver in a pulsed laser backscattering system. Assuming background noise, internal sensor noise and dark currents are negligible, the SNR can be determined by the signal-induced shot noise and is given by Hickman et al (1991) as

$$SNR = \sqrt{N_{pe}} \quad (5)$$

N_{pe} is the signal produced by the Brillouin return. Table 2.1 contains a summary of theoretical precision requirements of Brillouin shift measurements in respect to desired accuracy of sound speed measurements. It also gives the required SNR. The numbers in table 2.1 have been calculated using equations 3, 4 and 5 for a Brillouin shift of 7.5 GHz and sound speed of 1500 m/s. Given the assumptions above, the SNR figures clearly represent an ideal case.

Table 2.1: Summary table of theoretical accuracy requirements of Brillouin shift with respect to desired precision of sound speed measurements.

Required sound speed precision (m/s)	Uncertainty in Brillouin shift (Hz)	Resultant SNR
10	5.0E+07	10
1	5.0E+06	100
0.1	5.0E+05	1.0E+3
0.01	5.0E+04	1.0E+4
0.001	5.0E+03	1.0E+5

The expression for the number of Brillouin photoelectrons generated by an optical detector of a Brillouin lidar is stated in Hickman et al (1991) as

$$N_{pe} = N_1 \sigma_B \Delta z d\Omega \epsilon_{pm} \epsilon_{os} T_\lambda^2, \quad (6)$$

where:

- N_{pe} = number of Brillouin photoelectrons generated by the optical receiver,
- N_1 = number of laser photons transmitted,
- σ_B = Brillouin backscatter coefficient at $\theta = 180^\circ$,
- Δz = range resolution,
- $d\Omega$ = solid angle of receiver = $A_d / (z + nH_r)^2$,
- n = refractive index of seawater,
- z = depth in metres,
- A_d = area of detector,
- H_r = altitude of receiver in air (metres),
- ϵ_{pm} = efficiency of photomultiplier tube at laser wavelength,
- ϵ_{os} = efficiency of total optical system including instrumentation for measuring frequency separation,
- T_λ = transmission of light through water at laser wavelength = $\exp(-\gamma z)$,
- γ = "effective" attenuation coefficient, depending on receiver field of view. For small field of view γ equals beam attenuation coefficient (c) and wide field of view γ approaches diffuse attenuation coefficient (k).

2.3 Brillouin Measurement Techniques

A summary of experimental work to measure Brillouin scattering is given in table 2.2. This lists some of the initial experiments conducted by researchers to measure Brillouin scattering in liquids. The table primarily contains measurement techniques suitable for spontaneous Brillouin scattering, the mechanism that is most easily applied to remote sensing. Most of the early experiments have been conducted in laboratories. The main emphasis here has been to prove the existence of the Brillouin scattering mechanism in liquids. Later papers have tended to study the application of Brillouin scattering as a remote-sensing tool for measuring water properties.

Table 2.2: Summary table of experiments to measure spontaneous Brillouin scattering.

Author	Sample	Environment	Probing Technique	Detection Technique	Accuracy
Xiao et al (2000)	Pure Water	Laboratory	Pulsed ND:YAG laser operating at 532 nm.	Non-scanning spectroscopic detection technique.	The sound speed measured to an approximate accuracy of ± 0.75 m/sec.
Yves Emery and Edward S. Fry (1997)	Water sample. Purity not stated. Scattering measured at 175°.	Laboratory	Pulsed ND:YAG laser operating at 532 nm.	Scanning Fabry-Perot etalon and photomultiplier. Also describes development of a non-scanning spectroscopic detection technique.	Not reported
J. G. Hirschberg and J. D. Bryne (1984)	Shipping channel water and pure water.	Field and laboratory	0.1 Watt Argon ion laser operating at 488 nm in field experiments. Argon ion laser in laboratory.	Scanned Fabry-Perot interferometer in field. A dual Fabry-Perot non-scanning technique in lab space.	A deduced temperature measurement from field experiment is quoted to be $34 \pm 4^\circ\text{C}$.
Donald J. Collins et al (1984)	Distilled water at temperatures ranging from 0 – 30°C. Scattering angle of 175°.	Laboratory	Continuous wave Argon Ion laser operating at 514 nm.	Piezoelectric controlled Fabry-Perot interferometer and photomultiplier.	Temperature has been measured to an accuracy of $\pm 0.3^\circ\text{C}$. The sound speed measured to an approximate accuracy of ± 1 m/sec.
Arthur R. Maret and Ernest Yeager (1972)	Various electrolyte solutions. Scattering angle of 45°.	Laboratory	Continuous wave Argon Ion laser operating at 488 nm.	Piezoelectric interferometer and cooled phototube and photon counter.	Not reported
C. Leonard O'Connor and Joseph P. Schlupf (1967)	Pure Water at various temperatures. Scattering measured at 90°.	Laboratory	Continuous wave Helium Neon laser operating at 632.8 nm.	Scanned Fabry-Perot interferometer and photomultiplier tube.	Not reported
R. Y. Chiao and B. P. Stoicheff (1964)	Brillouin scattering measured at 165°20' for pure water at 20° C and other samples.	Laboratory	Continuous wave Helium Neon laser operating at 632.8 nm.	Fabry-Perot interferometer and photomultiplier.	Brillouin shift measured with an accuracy of $\pm 0.1\%$.

Author	Sample	Environment	Probing Technique	Detection Technique	Accuracy
G.B. Benedek et al (1964)	Brillouin scattering measured at 90° for pure water at 22.9 °C and other samples.	Laboratory	Continuous wave Helium Neon laser operating at 632.8 nm.	12 m focal length grating spectrograph and photomultiplier.	Brillouin shift measured with an accuracy of $\pm 0.5\%$. Hypersonic sound speed velocity with an accuracy of ± 10 m/sec.

The popularity of Fabry-Perot interferometers used by the researchers comes from the resolution required for measuring Brillouin scattering. An experimental configuration for measuring the Brillouin shift using a Fabry-Perot interferometer is shown in Figure 2.3. The earliest laser measurements of sound velocities from Brillouin scattering were made by probing a scattering medium with a continuous wave (CW) laser beam. Conventional optics was used to collect the scattered light at various angles. The most common method for resolving the scattered light into measurable frequency components was to pass it through a Fabry-Perot interferometer. The Fabry-Perot interferometer was usually coupled to an output device such as a photomultiplier tube, which amplifies the incoming signal. A spectrum from the scattered light could then be viewed and recorded for further analysis.

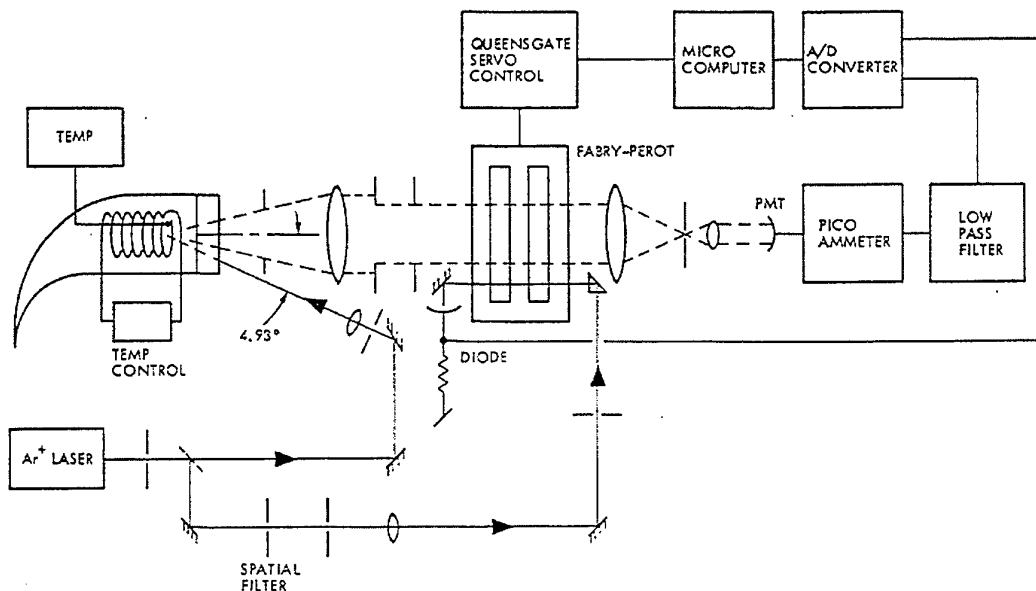


Figure 2.3: Experimental configuration reported by Collins et al (1984) for measuring Brillouin scattering in water.

2.4 Remote Sensing of Brillouin Scattering

The remote sensing of Brillouin scattering in water requires the use of pulsed lasers and time resolved signal detection. Pulsed lasers must be used to get a back-scattered

return that has depth resolution. The speed of light through a medium is a function of the refractive index of the medium. Time resolved signal detection is used synchronously with a pulsed laser system to track or collect information from a specific pulse and hence a specific depth. The duration of the light pulses determines depth resolution.

The laser options for time resolved measurements are mainly dye lasers or pulsed solid state lasers. Dye lasers and solid state lasers are appropriate choices for remote sensing because they can be optically pumped. This has implications for the size of a solid state laser system, since a reasonably small cavity and gain medium can be made to lase with a diode laser as a pump source. Gas lasers generally require electrical energy as a pump source to reach lasing threshold therefore requiring high voltage power supplies.

The blue-green spectrum of visible light has better transmission properties in water. Hence the most appropriate laser wavelengths for remote sensing are between 400 – 550 nm.

For typical sound speeds in seawater Brillouin doublets are spaced from the main laser line by approximately 7 – 8 GHz. For a range resolution of 1 metre, a lidar system will need to use 10 ns pulses. Recording and measuring the Brillouin frequency shift at 10 ns intervals is a demanding requirement for a measurement system. In the laboratory, environmental conditions can be controlled. Experimental parameters such as optical path length of a laser beam, the orientation and position of liquid samples with respect to the laser beam can be well defined. An optical table allows the use of high-resolution detection instrumentation such as Fabry-Perot interferometers. The Fabry-Perot needs to be operated in slow scanning mode to spectrally resolve the two Brillouin peaks. In a field-deployable system a scanning Fabry-Perot interferometer would not be suitable as it would suffer from noise caused by vibration. Non-scanning detection systems must be used in a field-deployable Brillouin lidar. Hirschberg et al (1984) reports a non-scanning technique using dual Fabry-Perots and a Michelson interferometer. Figure 2.4 contains a diagram of a non-scanning dual Fabry-Perot technique.

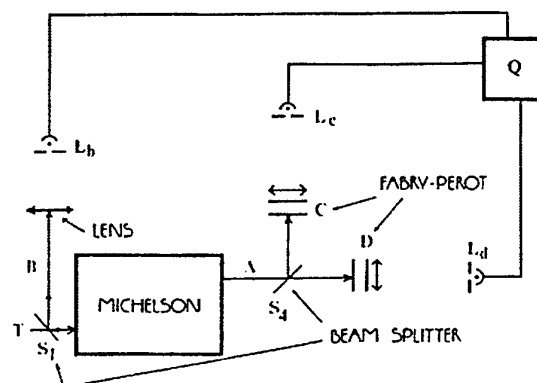


Figure 2.4: A block diagram taken from Hirschberg et al (1984). Dual Fabry-Perot arrangement implemented as a non-scanning technique for measuring Brillouin shift.

The configuration from Hirschberg et al (1984) is used to measure turbidity as well as the Brillouin shift. Light enters the arrangement at point T and is passed into a Michelson interferometer. The Michelson interferometer is configured to pass two beams out. Beam A has the elastically scattered light filtered out and passes the Brillouin doublets. Beam B consists of the elastically scattered light only. Photomultiplier L_b is used to measure the signal strength of Beam B, which is proportional to the particulate (turbidity) concentration of a water sample. Beam A is then directed into Fabry-Perots C and D. Both Fabry-Perots are locked to filter half of the total Brillouin shift. According to Hirschberg Fabry-Perot C is locked to filter the greater shift corresponding to higher sound speeds and Fabry-Perot D is locked to filter shifts corresponding to slower sound speeds. The output from the two Fabry-Perot interferometers is measured by photomultiplier tubes L_c and L_d . The speed of sound is measured by Q which is a signal processor unit that takes a ratio of the signals output from L_c and L_d . Figure 2.5 contains the theoretical pass bands of the Fabry-Perots and Michelson output of Beam A.

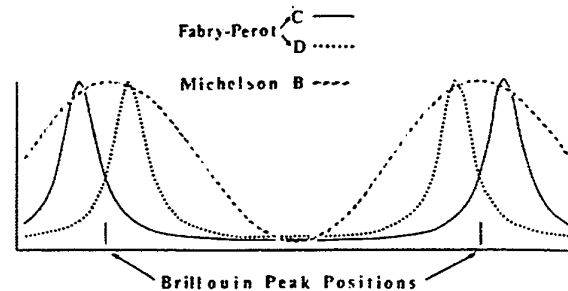


Figure 2.5: This figure represents pass bands for the three interferometers for measuring Brillouin shift. This figure is reported in Hirschberg et al (1984).

Emery and Fry (1997) have reported on work to establish a non-scanning spectroscopic detection system for an airborne Brillouin lidar. This detection system will use specific molecular absorption lines to block the main laser line and pass the Brillouin doublets. This is given in Figure 2.6.

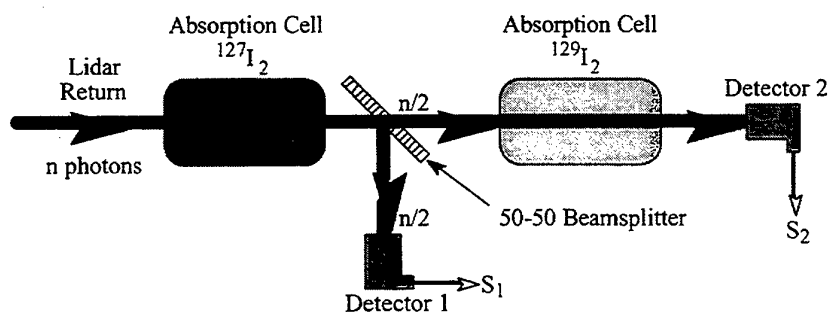


Figure 2.6: Diagram of Edward S Fry's spectroscopic technique using molecular absorption lines of vapour cells $^{127}\text{I}_2$ and $^{129}\text{I}_2$, Edward S Fry (1999).

The lidar return is collimated and directed into the $^{127}\text{I}_2$ cell, which absorbs the elastically scattered line and passes the Brillouin doublets. As the beam emerges

from the first cell (blocking filter), it is split so that half of its energy is directed onto a photodiode S_1 . The rest of the beam is directed into the edge filter $^{129}\text{I}_2$. Any change in the Brillouin shift results in a change of the effective transmission properties experienced by the light propagating through the cell. Specifically, as the Brillouin shift increases for higher sound speeds the transmission increases and vice versa for lower sound speeds. The output from the edge filter is measured with detector S_2 . Taking a ratio S_2/S_1 gives a value that is proportional to the Brillouin shift and sound speed. Results from using this detection technique can be found in Figure 2.7.

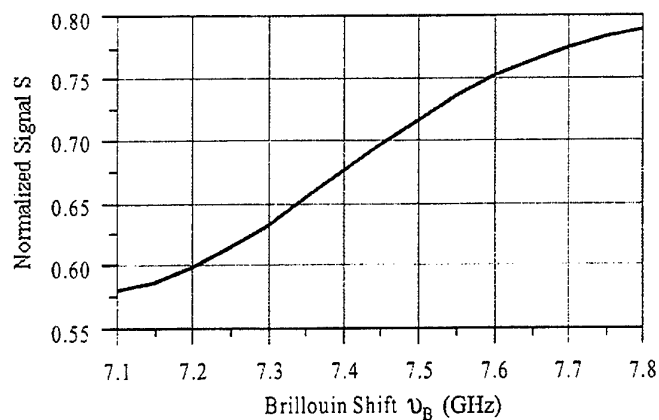


Figure 2.7: Results taken Edward S Fry (1999). 7.1 GHz corresponds to approximately 1420 m/s. 7.8 GHz corresponds to approximately 1560 m/s.

The results shown in figure 2.7 are of experiments conducted in the laboratory to demonstrate the concept of using the spectroscopic technique in detecting Brillouin shift. They show the relationship between the ratio and Brillouin shift and the range of sound speed that can be measured with this detection technique.

Fry and Emery have reported a conceptual airborne Brillouin lidar system which is shown in Figure 2.8. The second harmonic of a pulsed ND: Yag laser is used to probe a water column. The seed laser controls the output of the probe laser wavelength. The seed laser is controlled via locking electronics, which set the seed laser to a strong absorption line of the blocking filter. The backscattered return is collected by a telescopic lens that collimates the light and couples it into the Brillouin shift detection system, which is configured the same as that described in Figure 2.6. SHG refers to second harmonic generation. Ms are mirrors, BS are beam splitters, and PD is a photo diode used for feedback into the locking electronics. The acquisition system measures the output from photodetectors S_1 and S_2 .

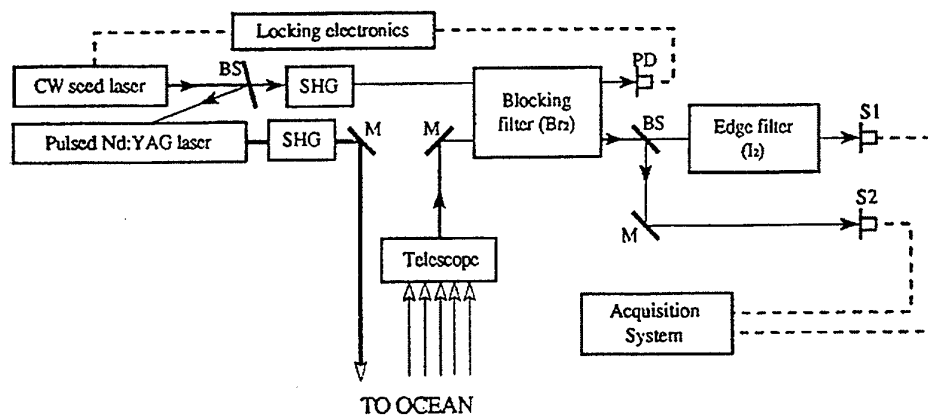


Figure 2.8: Schematic of Brillouin lidar system reported to be under development by Emery and Fry (1997).

3. Raman Scattering

3.1 The Raman Scattering Process

Raman scattering can be used to measure the temperature of a water sample. A temperature measurement from the Raman spectrum of ocean water coupled with historical figures of salinity could be used to predict the velocity of sound through ocean water. If Raman scattering is measured using a range resolved system, then the temperature profile characteristic can be determined for a column of water. This may have application for airborne and submerged platforms. An airborne platform would be able to rapidly profile the temperature of water sites and could be used in a similar way to the Laser Airborne Depth Sounder (LADS) or could be used to detect submarine-induced internal waves. With adequate precision in the temperature measurement, a maritime or airborne platform could use such a system to map or track thermoclines in water.

Raman scattering is a result of light interaction with rotational and vibrational molecular spectra. Specifically, it results from the interaction of light with vibrational-rotational spectra of the monomer and polymer forms of water. The polymer consists of water molecules that are weakly bonded with other water molecules. The monomer consists of unbound water molecules, one with an unbound H-atom and the other with an unbound O-atom. An illustration of the Raman return from the two water species is given in Figure 3.1.

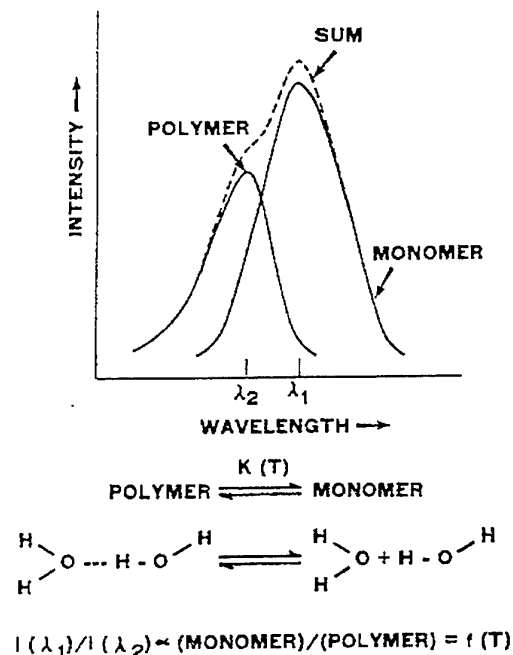


Figure 3.1: Illustration of Raman spectrum from Leonard et al (1979).

The spectrum is the sum of two spectral shifts caused by the monomer and polymer. The spectral shift comes from light being absorbed by polymer and monomer water molecules and then being re-emitted at lower energies. The energy of the light being re-emitted by the water molecules corresponds to their molecular rotational-vibrational spectra.

The amplitudes of the monomer and polymer spectra are proportional to their concentrations. The chemical equilibrium between the monomer and polymer is a function of temperature. As temperature increases the weak bonds between polymer water molecules break and become independent monomer water molecules. This changes the proportions of polymer and monomer water, which are reflected in the Raman spectrum as a change in amplitude of the polymer and monomer components. Taking a ratio of polymer to monomer amplitudes in a Raman spectrum gives the temperature of a water sample.

Collins et al (1984) has presented a curve relating the Raman centre line to the excitation wavelength.

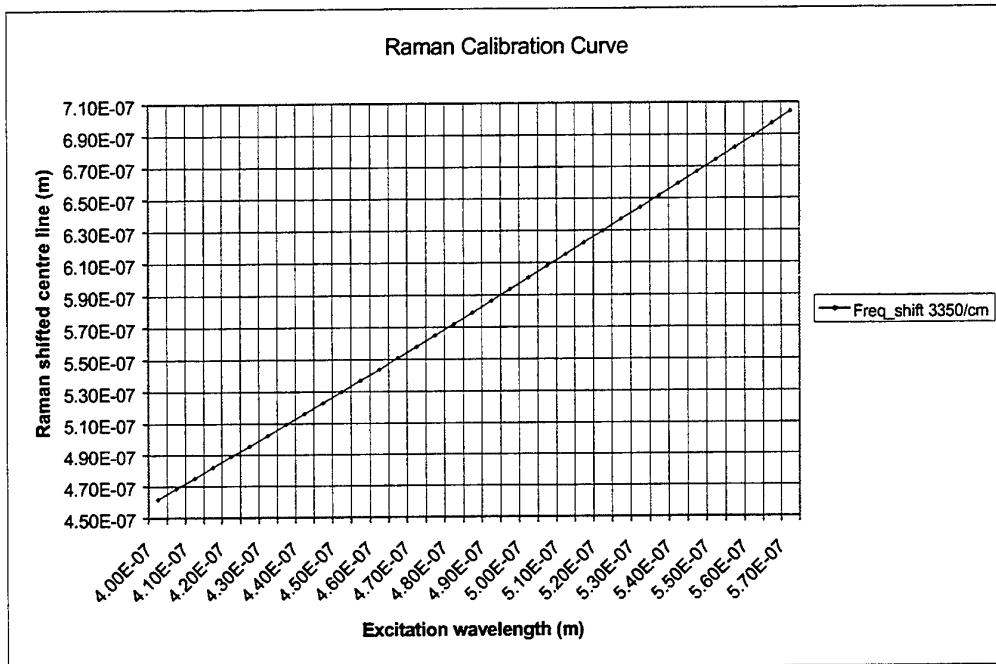


Figure 3.2: Raman calibration curve calculated assuming shift of 3350 wavenumber/cm ($\Delta\nu$). Raman shifted centre line is calculated with the expression $\Delta f = c\Delta\nu/100$. The Raman shifted wavelength has a longer wavelength than the excitation laser.

3.2 Raman Measurement Techniques

There are two main techniques for measuring Raman scattering in water. They are known as the two-colour technique and the depolarisation technique.

3.2.1 Two-colour Technique

Light from a monochromatic source is directed into a sample of water. Conventional optics is used to collect the Raman backscattered light. The Raman spectrum is passed through a spectral resolving device to resolve monomer and polymer components. The output from a spectral resolving device is then passed through a photomultiplier to measure the amplitude of the polymer and monomer components. The temperature of the water sample is measured by taking a ratio of polymer to monomer amplitudes.

A block diagram of a Raman lidar that incorporates the two-colour detection technique is given in Figure 3.3.

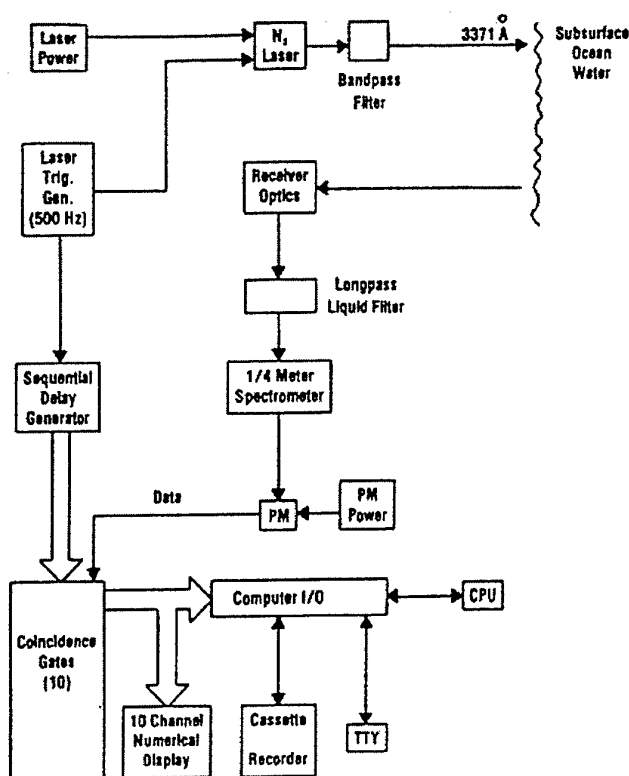


Figure 3.3: A block diagram of the Raman lidar system reported in Leonard et al (1979).

Collins et al (1984) has reported that the ratio from the two-colour method is linearly dependent on temperature, but is also a function of salinity. Collins has related the two-colour intensity ratio to the temperature (T) and salinity (S) with the expression,

$$R = r_0 + r_1 T + r_2 S + r_3 S^3 \quad (7)$$

Where R is the two-colour ratio, $r_0 = 0.555$, $r_1 = 5.58 \times 10^{-3}$, $r_2 = 4.496 \times 10^{-3}$, $r_3 = -4.58 \times 10^{-5}$. R is a dimensionless quantity. Figure 3.4 contains results presented in Collins et al (1984) that describe the relationship between the two-colour ratio and temperature. It is not clear from Collins et al (1984) why the lines presented in Figure 3.4 have different gradients. The fit of the lines with respect to their data suggests that the difference in gradients may be attributed to the specific experimental configurations used by the two research groups.

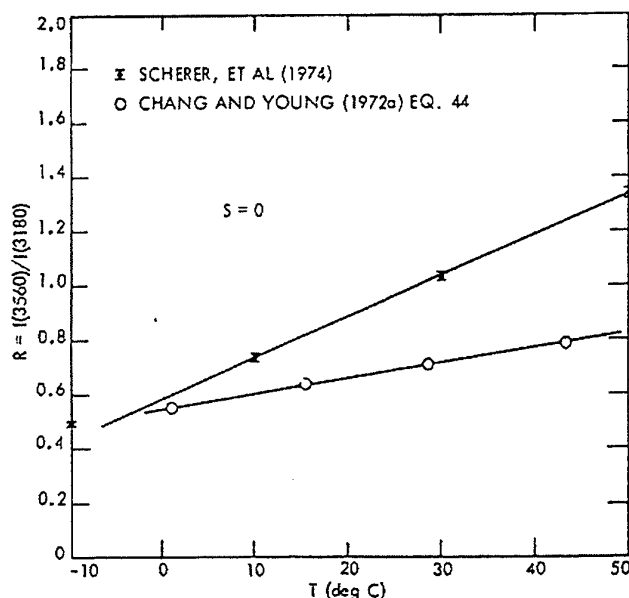


Figure 3.4: Results presented in Collins et al (1984) of pure water. Ratio of Raman intensity at two wavelengths with respect to temperature.

The two-colour method has an accuracy limitation due to spectral attenuation coefficients of water. The attenuation coefficients for the central wavelengths that define monomer and polymer concentrations vary in magnitude. Chang (1975) and Leonard (1983) have derived an expression relating the difference in attenuation coefficients to the uncertainty in measured temperature

$$\Delta T(^{\circ}\text{C}) = 100\Delta kx. \quad (8)$$

Where Δk is the difference in attenuation coefficients and x is depth in metres. A transmissometer has been used to measure the attenuation coefficients of a number of wavelengths in tropical waters off Thursday Island, Queensland. At one of the water sites the attenuation coefficient at 440 and 455 nm were measured to be 0.225 and 0.2 per metre respectively. If these wavelengths were to correspond to the spectral centre lines of monomer and polymer components, the uncertainty in measured temperature from equation 8 would rise to 10 $^{\circ}\text{C}$ after four metres of propagation.

3.2.2 Depolarisation Technique

Linear or circularly polarised light from a monochromatic source is directed into a sample of water. The Raman backscattered light is collected using conventional optics coupled with polarisation analysers. A light beam undergoes a Raman shift when interacting with polymer and monomer water. However the polymer and monomer also have an effect on the polarisation state of the Raman scattered return. The polymer will produce Raman returns with a different polarisation state to the launched state while the monomer returns will have the same polarisation as the launched state. Therefore the polarisation of a Raman spectrum can be used to discriminate polymer and monomer concentration levels. Chang and Young (1975)

and Collins et al (1984) have measured the depolarisation ratio as $I_{\text{perpendicular}}/I_{\text{parallel}}$. Chang and Young (1975) state that the depolarisation ratio decreases with increasing temperature. As temperature increases the concentration of polymer water decreases and monomer increases therefore the depolarisation ratio provides a measure of the water temperature.

Collins et al (1984) has reported that circular polarisation is preferred to linear polarisation because the depolarisation ratio is more sensitive to temperature and offers a greater statistical accuracy for measuring the weaker depolarised component. Leonard and Sweeney (1988) have reported that salinity can be measured from the rate of change of the polarisation ratio spectrum with wavelength. This could potentially turn a Raman lidar into a complete stand-alone forecast system for velocity and temperature profiles.

A schematic of a system from Chang and Young (1975) utilising the depolarisation method is shown in Figure 3.5. Laser light is directed through a filter which blocks stray radiation at UV and Raman wavelengths and is right hand circularly polarised by a linear polariser and quarter wave plate. The left and right handed backscattered Raman returns are converted by a quarter wave plate to two linearly polarised components, which are separated by a polarising beam splitting cube. Another interference filter is used to block stray backscatter from the probe laser wavelength. Two photomultiplier tubes are used to measure the two polarised return components that produce $I_{\text{perpendicular}}$ and I_{parallel} .

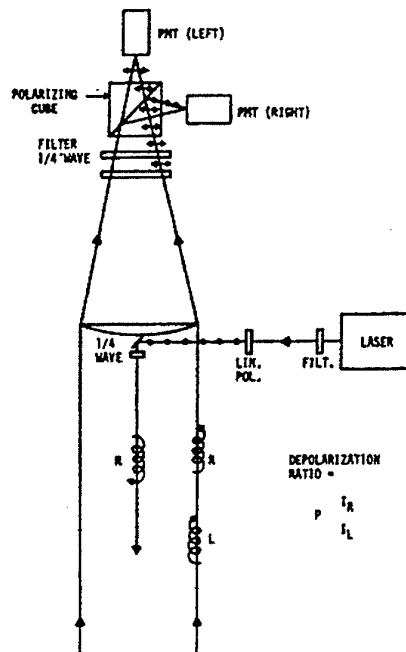


Figure 3.5: Schematic of depth resolved Raman lidar using the circular polarisation method. This system was proposed by Chang and Young (1975).

3.3 Precision and Sensitivity

Leonard (1979) has reported that the ratio of the polymer to monomer concentration using the two-colour technique changes by one percent per degree centigrade. Chang and Young have reported a ratio sensitivity of one percent per degree centigrade using the circular depolarisation technique. Both references suggest that measured temperature accuracy depends upon the number of Raman photoelectrons sampled every measurement.

Based on a ratio sensitivity of 1%/°C Liu et al (1992) has derived an expression relating the uncertainty in measured temperature to the SNR.

$$\Delta T = \frac{100}{SNR} \approx \frac{100}{\sqrt{N_{pe}}} \quad (9)$$

This assumes that background noise from the environment and sensor internal noise and dark currents are negligible. Then the SNR can be determined by the signal-induced shot noise and is given as the square root of N_{pe} . N_{pe} is the number of Raman photoelectrons produced by a Raman lidar with every back-scattered return. The required precision in measured temperature determines the number of photoelectrons that need to be generated by an optical detector of a Raman lidar. This is described in table 3.1. The numbers presented in table 3.1 have been calculated using equation 9. The SNR numbers apply to the weaker of the two components in both techniques. In the two-colour technique we use the photons from the water species that has the smaller concentration. In the depolarisation technique we use the number of photons returning depolarised from the launched state of polarisation.

Table 3.1: Summary table of Raman photoelectrons required for specific temperature precision.

Required precision (°C)	Resultant SNR
10	10
1	100
0.1	1.0E+3
0.01	1.0E+4
0.001	1.0E+5

The expression for the number of Raman photoelectrons generated by an optical detector of a Raman lidar system is stated in Leonard et al (1979) as

$$N_{pe} = N_{laser} N_{scat} \sigma_{Raman} \Delta R \frac{\Omega}{n^2} \epsilon_{pe} \epsilon_{op} T_{\lambda 1} T_{\lambda 2} \quad (10)$$

Where,

- N_{pe} = number of Raman photoelectrons generated per pulse,
- N_{laser} = number of laser photons transmitted per pulse,
- N_{scat} = density of molecular scatterers of a given species,

- σ_{Raman} = Raman scattering cross section per particle per steradian,
 ΔR = range resolution in metres,
 Ω = detection solid angle of collector,
 n = refractive index of water,
 ϵ_{pe} = photocathode photoelectric efficiency,
 ϵ_{op} = optical system efficiency,
 $T_{\lambda 1}$ = Two way transmission at laser wavelength,
 $T_{\lambda 2}$ = Two way transmission at Raman wavelength.

3.4 Summary of Reported Results

A summary of some previous work for temperature measurements using Raman scattering is presented in table 3.2 below.

Table 3.2: Summary table of experiments to measure Raman scattering.

Author	Sample	Environment	Probing Technique	Detection Technique	Accuracy
Becucci et al (1999)	Pure water and various salt concentrations	Laboratory	CW Argon @ 514 nm and ND: YAG @ 354.7 nm	Two-colour technique	Not reported
John Bell (1994)	Various water samples	Laboratory and field.	CW Argon ion @ 514 in lab space, pulsed dye laser @ 308 & 480 nm in field	Two-colour technique	Claims to measure temperature with accuracy of $\pm 0.01^\circ\text{C}$.
Liu et al (1992)	Sea water	Laboratory and field.	Pulsed ND: YAG laser @ 532 nm	Two-colour technique	Laboratory test $\pm 0.4^\circ\text{C}$, field test $\pm 0.5^\circ\text{C}$.
Collins et al (1984)	Distilled water	Laboratory	Pulsed dye laser @ 460 nm	Depolarisation technique	Propose measurement accuracy using Two-colour technique $\pm 0.53^\circ\text{C}$, depolarisation technique yields $\pm 0.85^\circ\text{C}$
Leonard and Caputo (1983)	Water column	Water tank	Pulsed dye laser @ 470 nm	Depolarisation technique	Reported accuracy of $\pm 0.5^\circ\text{C}$.
Leonard et al (1979)	Open ocean, various locations	Field	Pulsed Nitrogen laser operating at 371.1 nm. 10 ns pulses at 500 Hz repetition	Two-colour technique. Blocking filter for main laser line scanning spectrometer and photomultiplier	Reported accuracy of $\pm 1^\circ\text{C}$.
Leonard et al (1977)	Tidal estuary (Annisquam river)	Field	Pulsed Nitrogen laser operating at 371.1 nm. 10 ns pulses at 500 Hz repetition	Two-colour technique. Scanning spectrometer and photomultiplier	Initial field experiment accuracy of $\pm 2^\circ\text{C}$.
Chang and Young (1975)	Aqueous solution of NaCl 40 %.	Laboratory	460 nm right handed circularly polarised (RHCP) laser beam	Depolarisation technique.	Propose measurement accuracy of $\pm 0.5^\circ\text{C}$.

3.5 Remote Sensing of Raman Scattering

Range resolved measurements of Raman scattering will require the use of a pulsed laser and a time-resolved detection system to discriminate between return pulses from different water depths. Most authors have reported using excitation wavelengths ranging from the ultra-violet (UV) to the visible blue-green. The advantage of using wavelengths in the UV is that the Raman shifted return is at blue-green wavelengths, which are the least attenuated in water. Additionally the visible spectrum beyond the blue-green can be filtered out to avoid high background radiance. The main disadvantage of using blue-green *excitation* wavelengths is that the Raman shifted return lies in the yellow-red. In the yellow part of the visible spectrum, the background radiance levels are quite high due to solar reflection. Such high background radiance can lower the signal to noise ratio, which increases the uncertainty in measuring the concentrations of polymer and monomer from the Raman spectrum, thereby decreasing the precision of temperature measurements. To maximise the photon return from water the Raman spectrum should be made to experience the least attenuation. Buiteveld et al (1994) has published absorption and scattering coefficients for pure water over the spectral range of 300 to 800 nm. Buitevelde reports absorption coefficients of 0.0058 to 0.0238 per metre in the 400-500 nm range compared with absorption coefficients of 0.2 to 2.7 per metre in the 600-800 nm range.

The full width at half maximum (FWHM) of the Raman shift is approximately 20nm. The broad spectrum of the Raman return can contain significant background radiation, necessitating the use of appropriate filtering and background subtraction techniques. The circular depolarisation method is more suitable for greater depth penetration as the two-colour technique is limited by differential attenuation. This limitation increases the uncertainty in measured temperature with increasing depth.

Leonard (1979) presented an operational map for an airborne Raman system. The operational map is given in Figure 3.6. It presents temperature accuracies at specific photoelectron counts as a function of depth or attenuation length and a parameter, which is described as the map number M. The gradient of the lines is determined by the transmission loss as a function of depth. The operational map proposes a fundamental limit to the accuracy of measuring temperature of water using Raman scattering. Leonard has reported that due to what they have labelled as the Volume Depolarisation Limit, the best temperature accuracy achievable with a Raman lidar is 0.1°C.

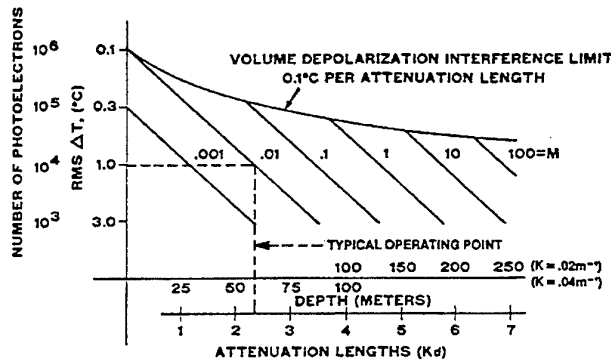


Figure 3.6: Raman lidar operational map taken from Leonard et al (1979). The typical operating point has been derived for a lidar system proposed in Leonard et al (1979). The map is for a system operating in the 100-m mixed layer.

The M number is defined by

$$M = \left(\frac{P_l}{20} \right) \left(\frac{\Delta h}{10} \right) \left(\frac{1}{R} \right)^2 T, \quad (11)$$

where P_l is the average laser power in watts, Δh is the range resolution in metres, R is the altitude of the aircraft in kilometres and T is the integration time of a measurement in seconds.

4. Conclusion

1. Brillouin and Raman scattering can be used to measure ocean sound velocity and temperature.
2. An absolute change in the sound velocity will produce an absolute shift in the Brillouin frequency. The precision of measuring the sound velocity of water using Brillouin scattering depends on the uncertainty in the measurement of the Brillouin shift. Authors have related the precision in measuring sound velocity by Brillouin scattering and temperature by Raman scattering to the number of photoelectrons sampled by the respective lidar systems. This ultimately depends on the number of Raman and Brillouin backscattered photons returning per pulse of a probe laser. The attenuation coefficient of the water at the Raman and Brillouin wavelengths and the energy of each laser pulse are the critical parameters determining the number of photons that will return per pulse. Researchers have reported measurement accuracies ranging from ± 0.75 m/s to ± 10 m/sec for measuring sound speed using Brillouin scattering and $\pm 0.4^\circ\text{C}$ to $\pm 2^\circ\text{C}$ for measuring temperature using Raman scattering.
3. The laser wavelength of a Brillouin lidar should be the one that suffers minimum attenuation through the waters that are to be studied.

4. The laser wavelength of a Raman lidar should be the one that has a Raman shift into a wavelength band of least attenuation through waters that are to be studied.
5. Non-scanning frequency detection techniques for resolving Brillouin shift will have to be used for a field-deployable Brillouin lidar to allow sufficient time to process successive laser pulses.
6. The depolarisation technique should be used in a field-deployable Raman lidar for higher temperature precision at greater depths.

5. References

Arthur R. Maret and Ernest Yeager, (1972), "Rayleigh-Brillouin intensity ratios in aqueous electrolyte solutions", *Journal of Chemical Physics* Volume 59, Number 1, pp. 206-212.

John Bell, (1994) "Flying lidar monitors undersea temperature", *OLE* September, pp. 21-24.

C. Leonard O'Connor and Joseph P. Schlupf, (1967), "Brillouin scattering in water: The Landau-Placzek ratio", *Journal of Chemical Physics* Volume 47, Number 1, pp. 31-38.

Chin H. Chang and Lee A. Young, (1975), "Remote measurement of ocean temperature from depolarisation in Raman scattering", *The use of lasers for hydrographic studies*, NASA SP-375, NASA Wallops Station, pp. 105-112.

D. A. Leonard, B. Caputo and R. L. Johnson, (1977) "Experimental remote sensing of subsurface temperature in natural ocean water", *Geophysical Research Letters*, Volume 4, Number 7, pp. 279-281.

D. A. Leonard, B. Caputo and F. E. Hoge, (1979), "Remote sensing of subsurface water temperature by Raman scattering", *Applied Optics*, Volume 18, Number 11, pp. 1732-1745.

Donald A Leonard and Bernard Caputo, (1983), "Raman remote sensing of the ocean mixed-layer depth", *Optical Engineering*, Volume 22, Number 3, pp. 288-291.

Donald A. Leonard and Harold E. Sweeney, (1988), "Remote sensing of ocean physical properties: a comparison of Raman and Brillouin techniques", *Ocean Optics IX*, SPIE Volume 925, pp. 407-414.

Donald J. Collins, John A. Bell, Ray Zanoni, I. Stuart McDermid, James B. Breckinridge, Cesar A. Sepulveda, (1984), "Recent progress in the measurement of temperature and salinity by optical scattering", *Ocean Optics VII*, SPIE Volume 489, pp. 247-269.

Edward S. Fry, (1999), "Lidar profiling of sound speed and temperature in the ocean upper mixed layer",
<http://www.onr.navy.mil/oas/info/yerpts/poye98/pofes.pdf>.

G. B. Benedek, J. B. Lastovka, K. Fritsch and T. Greytak, (1964), "Brillouin scattering in liquids and solids using low-power lasers", *Journal of Optical Society of America*, Volume 54, pp. 1284-1285.

G. Daniel Hickman, John M. Harding, Michael Carnes, Al Pressman, George W. Kattawar and Edward S. Fry, (1991), "Aircraft laser sensing of sound velocity in water: Brillouin scattering", *Remote Sensing Environment*, 36, pp. 165-178.

Gangyao Xiao, Jeffrey Katz, Edward S. Fry, (2000), "Sound speed measurement with an edge technique", CLEO 2000 Technical Digest Vol 39, pp. 494-495.

H. Buiteveld, J.H.M. Hakvoort and M. Donze, (1994), "The optical properties of pure water", Ocean Optics XII, SPIE Volume 2258, pp. 174-183.

J. G. Hirschberg and J. D. Bryne, (1984), "Rapid underwater ocean measurements using Brillouin scattering", Ocean Optics VII, SPIE Volume 489, pp. 270-276.

Joseph G. Hirschberg, Alain W. Wouters and James D. Bryne, (1975), "Laser measure of sea salinity, temperature and turbidity in depth", Remote Sensing Energy Related Studies, Wiley and Sons, New York. pp. 157-167.

Liu Zhi-shen, Zhang Jin-long, Chen Wen-zhong, Huang Xiao-sheng and Ma Jun, (1992), "Remote sensing of subsurface water temperature using Raman lidar", Laser Radar VII, SPIE Volume 1633, pp. 321-329.

Maurizio Becucci, Stefano Cavalieri, Roberto Eramo, Lorenzo Fini and Marzia Materazzi, (1999), "Accuracy of remote sensing of water temperature by Raman spectroscopy", Applied Optics Volume 38, Number 6, pp. 928-931.

R. Y. Chiao and B. P. Stoicheff, (1964), "Brillouin scattering in liquids excited by the He-Ne maser", Journal of Optical Society of America, Volume 54, pp. 1286-1287.

Yves Emery and Edward S. Fry, (1997), "Laboratory development of a lidar for measurement of sound velocity in the ocean using Brillouin scattering", Ocean Optics XIII, SPIE Volume 2963, pp. 210-215.

6. Bibliography

Bruce R. Marshall and Raymond C. Smith, (1990), "Raman scattering and in-water ocean optical properties", *Applied Optics*, Volume 29, Issue 1, pp. 71-84.

Chuanmin Hu and Kenneth J. Voss, (1997), "In situ measurements of Raman scattering in clear ocean water", *Applied Optics* Volume 36, Number 27, pp. 6962-6967.

Donald A. Leonard, (1981), "Remote Raman measurement techniques", *Optical Engineering*, Volume 20, Number 1, pp. 90-94.

Donald A. Leonard and Harold E. Sweeney, (1990), "A comparison of stimulated and spontaneous laser radar methods for the remote sensing of ocean physical properties", *Ocean Optics X, SPIE Volume 1302*, pp. 568-582.

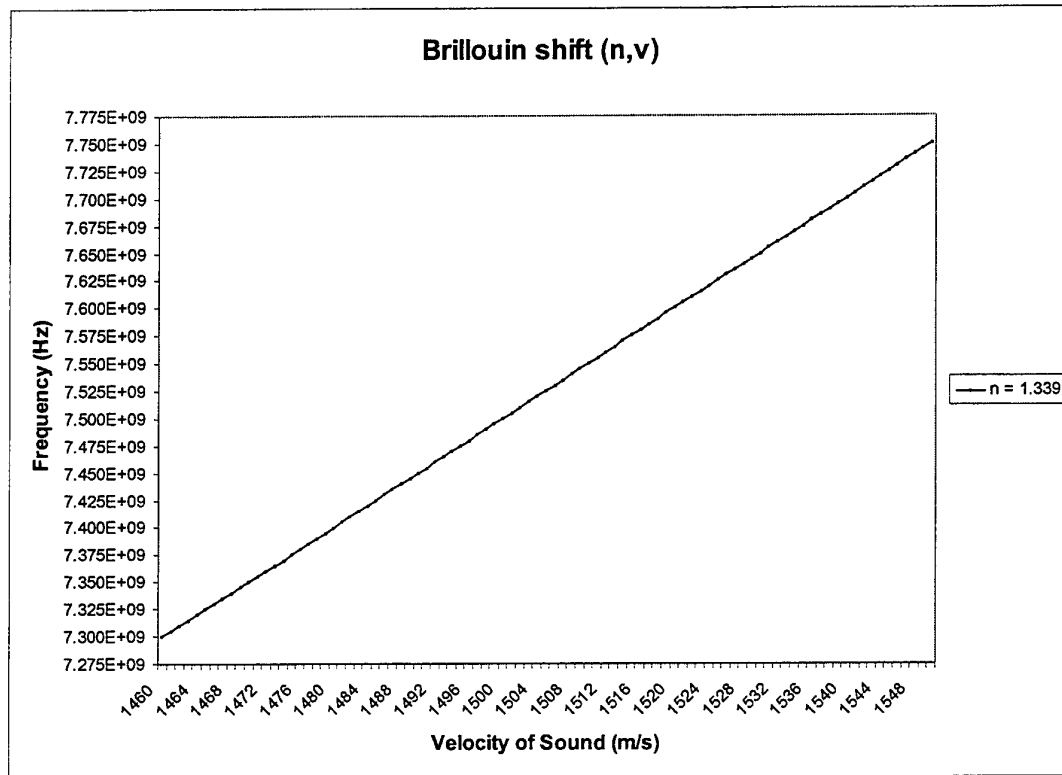
J. L. Guagliardo and H. L. Dufilho, (1980), "Range-resolved Brillouin scattering using a pulsed laser", *Review of Scientific Instruments* Volume 51, pp. 79-81.

Jasmine S. Bartlett, Kenneth J. Voss, Shubha Sathyendranath and Anthony Vodacek, (1998), "Raman scattering by pure water and seawater", *Applied Optics* Volume 37, Number 15, pp. 3324-3332.

S. M. Pershin and A. F. Bunkin, (1999), "Detection of water heating by second harmonic ND: YAG laser pulses using spontaneous Raman scattering spectrum", *Optics and Spectroscopy* Volume 87, Number 3, pp. 376-379.

Robert Hans Stavn, (1990), "Raman-scattering effects at the shorter visible wavelengths in clear ocean waters", *Ocean Optics X, SPIE Volume 1302*, pp. 94-100.

Appendix A: Brillouin frequency shift



DISTRIBUTION LIST

Remote Sensing of Ocean Waters with Raman and Brillouin Scattering

Joyanto Mukerjee

AUSTRALIA

DEFENCE ORGANISATION

Task Sponsor:

COMAUSNAVSUBGRP ATTN: CSO (Cap Dev)

S&T Program

Chief Defence Scientist	}	shared copy
FAS Science Policy		
AS Science Corporate Management		
Director General Science Policy Development		
Counsellor Defence Science, London (Doc Data Sheet)		
Counsellor Defence Science, Washington (Doc Data Sheet)		
Scientific Adviser to MRDC Thailand (Doc Data Sheet)		
Scientific Adviser Policy and Command		
Navy Scientific Adviser (Doc Data Sheet and distribution list only)		
Scientific Adviser - Army (Doc Data Sheet and distribution list only)		
Air Force Scientific Adviser		
Director Trials		

Aeronautical and Maritime Research Laboratory

Director		
Chief of Maritime Operations Division	}	shared copy
Research Leader Maritime Sensor Systems		
Head Maritime Optronics Group		
Mr Trevor Adams, MOD		
Mr Stuart Sutherland, MOD		
Mr Joyanto Mukerjee, MOD (3 copies)		
Dr Phillip Chapple MOD		
Dr Steve Galea AED		

DSTO Library

Library Fishermans Bend (Doc Data sheet only)
Library Maribyrnong (Doc Data sheet only)
Library Salisbury
Australian Archives
Library, MOD, Pyrmont (Doc Data sheet only)
Library, MOD, HMAS Stirling
US Defense Technical Information Centre, 2 copies
UK Defence Research Information Center, 2 copies
Canada Defence Scientific Information Service, 1 copy
NZ Defence Information Centre, 1 copy

Capability Systems Staff

Director General Maritime Development (Doc Data Sheet only)

Director General Aerospace Development (Doc Data Sheet only)

Knowledge Staff

Director General Command, Control, Communications and Computers (DGC4)
(Doc Data Sheet only)

Director General Intelligence, Surveillance, Reconnaissance, and Electronic Warfare (DGISREW) R1-3-A142 CANBERRA ACT 2600 (Doc Data Sheet only)

Director General Defence Knowledge Improvement Team (DGDKNIT)
R1-5-A165, CANBERRA ACT 2600 (Doc Data Sheet only)

Navy

SO (SCIENCE), COMAUSNAVSURFGRP, BLD 95, Garden Island, Locked Bag 12, PYRMONT NSW 2009 (Doc Data Sheet and distribution list only)

DNC4ISREW, ATTN: DNISREWSG

DGMD, ATTN: DMD 1 copy

Army

Stuart Schnaars, ABCA Standardisation Officer, Tobruk Barracks, Puckapunyal, 3662 (4 copies)

SO (Science), Deployable Joint Force Headquarters (DJFHQ) (L), MILPO Gallipoli Barracks, Enoggera QLD 4052 (Doc Data Sheet only)

Intelligence Program

DGSTA Defence Intelligence Organisation

Manager, Information Centre, Defence Intelligence Organisation

Corporate Support Program

Library Manager, DLS-Canberra

UNIVERSITIES AND COLLEGES

Australian Defence Force Academy

Library

Head of Aerospace and Mechanical Engineering

Hargrave Library, Monash University (Doc Data Sheet only)

Librarian, Flinders University

OTHER ORGANISATIONS

NASA (Canberra)

AusInfo

OUTSIDE AUSTRALIA**ABSTRACTING AND INFORMATION ORGANISATIONS**

Library, Chemical Abstracts Reference Service

Engineering Societies Library, US

Materials Information, Cambridge Scientific Abstracts, US

Documents Librarian, The Center for Research Libraries, US

INFORMATION EXCHANGE AGREEMENT PARTNERS

Acquisitions Unit, Science Reference and Information Service, UK

Library - Exchange Desk, National Institute of Standards and Technology, US

SPARES (5 copies)

Total number of copies: 49

DEFENCE SCIENCE AND TECHNOLOGY ORGANISATION DOCUMENT CONTROL DATA				1. PRIVACY MARKING/CAVEAT (OF DOCUMENT)		
2. TITLE Remote Sensing of Ocean Waters with Raman and Brillouin Scattering			3. SECURITY CLASSIFICATION (FOR UNCLASSIFIED REPORTS THAT ARE LIMITED RELEASE USE (L) NEXT TO DOCUMENT CLASSIFICATION) <div style="display: flex; justify-content: space-between;"> Document U </div> <div style="display: flex; justify-content: space-between;"> Title U </div> <div style="display: flex; justify-content: space-between;"> Abstract U </div>			
4. AUTHOR(S) Joyanto Mukerjee			5. CORPORATE AUTHOR Aeronautical and Maritime Research Laboratory 506 Lorimer St Fishermans Bend Vic 3207 Australia			
6a. DSTO NUMBER DSTO-TN-0346		6b. AR NUMBER AR-011-826		6c. TYPE OF REPORT Technical Note		
			7. DOCUMENT DATE March 2001			
8. FILE NUMBER M9505/19/241		9. TASK NUMBER NAV 00/095		10. TASK SPONSOR COMAUSNAVSUBGRP		
			11. NO. OF PAGES 26		12. NO. OF REFERENCES 21	
13. URL on the Worldwide Web http://www.dsto.defence.gov.au/corporate/reports/DSTO-TN-0346.pdf					14. RELEASE AUTHORITY Chief, Maritime Operations Division	
15. SECONDARY RELEASE STATEMENT OF THIS DOCUMENT <p style="text-align: center;"><i>Approved for public release</i></p>						
OVERSEAS ENQUIRIES OUTSIDE STATED LIMITATIONS SHOULD BE REFERRED THROUGH DOCUMENT EXCHANGE, PO BOX 1500, SALISBURY, SA 5108						
16. DELIBERATE ANNOUNCEMENT No Limitations						
17. CASUAL ANNOUNCEMENT Yes						
18. DEFTEST DESCRIPTORS Brillouin scattering, Remote sensing, Raman scattering, Lidar						
19. ABSTRACT This document presents a literature survey on the remote sensing of ocean waters with Raman and Brillouin scattering. It explains the physical process involved for these scattering processes to occur in water and a description of techniques employed by researchers to exploit Raman and Brillouin scattering to measure temperature and sound velocity in water. The papers surveyed for this report present measurement accuracies ranging from ± 0.75 m/sec to ± 10 m/sec for measuring sound velocity using Brillouin scattering and ± 0.4 °C to 2 °C for measuring temperature using Raman scattering.						